

Article

High-Efficiency Perovskite Solar Cell with an Air-Processable Active Layer via Sequential Deposition

Shih-Han Huang^{1,2}, Chien-Te Tsou³, Yu-Hung Hsiao^{2,4}, Chia-Feng Li^{2,5}, You-Ren Chen³, Wei-Fang Su^{3,5,*} and Yu-Ching Huang^{1,2,3,*}¹ Center for Sustainability and Energy Technologies, Chang Gung University, Taoyuan 33302, Taiwan² Organic Electronics Research Center, Ming Chi University of Technology, New Taipei City 24301, Taiwan³ Department of Materials Engineering, Ming Chi University of Technology, New Taipei City 24301, Taiwan⁴ Department of Electronic Engineering, National Taiwan University of Science and Technology, Taipei 10607, Taiwan⁵ Department of Materials Science and Engineering, National Taiwan University, Taipei 10617, Taiwan* Correspondence: suwf@ntu.edu.tw (W.-F.S.); huangyc@mail.mcut.edu.tw (Y.-C.H.)**How To Cite:** Huang, S.-H.; Tsou, C.-T.; Hsiao, Y.-H.; et al. High-Efficiency Perovskite Solar Cell with an Air-Processable Active Layer via Sequential Deposition. *Materials and Sustainability* **2025**, *1*(1), 3. <https://doi.org/10.53941/matsus.2025.100003>.

Received: 4 December 2024

Revised: 26 December 2024

Accepted: 30 December 2024

Published: 2 January 2025

Abstract: The development of efficient, scalable, and low-cost photovoltaic technologies is critical for advancing global energy sustainability. Perovskite solar cells (PSCs) have emerged as promising alternatives to traditional single-junction silicon-based solar cells due to their high power conversion efficiency (PCE) and solution-processable active materials. However, conventional fabrication methods typically require inert environments and complex anti-solvent processes, which increase production costs and limit scalability. Sequential deposition offers a promising solution by decoupling the solidification and crystallization steps, thereby eliminating the need for anti-solvent processes. Despite these advantages, fabricating high-quality mixed-cation perovskite layers in air remains a significant challenge, primarily due to the sensitivity of perovskite materials to moisture, which disrupts phase stability and perovskite phase formation. In this study, we addressed these challenges by developing an air-processable perovskite layer using a sequential deposition process. To overcome moisture-induced issues, pre-heating the substrate was employed to reduce surface tension and improve film coverage. Furthermore, imidazole iodide (ImI) was introduced into the PbI_2 precursor to effectively cap Pb sites, preventing moisture interference and promoting a complete transition to the α -phase of formamidinium lead iodide (FAPbI₃) without residual PbI_2 in air. These strategies enabled the production of PSCs in air achieving a champion PCE of 18.73%. Stability testing further demonstrated that PSCs incorporating ImI exhibited a T_{80} device lifetime exceeding 500 h. The finding demonstrates its role in moisture prevention and durability enhancement for the air-processable perovskite solar cells.

Keywords: air-processable; mixed-cation; additive; sequential deposition; perovskite

1. Introduction

With increasing global attention on energy sustainability, the advancement of solar energy has become imperative. Perovskite solar cells (PSCs) have recently emerged as highly efficient candidates to compete with traditional single-junction silicon-based solar cells due to their impressive power conversion efficiency (PCE) and capability for solutions process. These features hold significant potential for enabling next-generation, low-cost photovoltaic technologies [1,2]. Perovskite materials, typically characterized by a tetragonal ABX_3 structure, consist of inorganic B-site compounds such as lead halides and organic A-site compounds like ammonium-based halides [3]. Effective mixing of these inorganic and organic components is crucial during the solidification from



Copyright: © 2025 by the authors. This is an open access article under the terms and conditions of the Creative Commons Attribution (CC BY) license (<https://creativecommons.org/licenses/by/4.0/>).

Publisher's Note: Scilight stays neutral with regard to jurisdictional claims in published maps and institutional affiliations.

solution. A commonly adopted strategy for optimizing perovskite crystallization is anti-solvent dripping method, which facilitates the formation of high-quality perovskite films [4,5]. While PSCs fabricated via the one-step anti-solvent method under inert nitrogen (N_2) environments can achieve high PCE, such complex processing are cost-intensive and unsuitable for large-scale production. This limitation underscores the importance of developing scalable, air-processable perovskite layers.

Fabricating perovskite layers in ambient air presents significant challenges, particularly due to the sensitivity of perovskite materials to moisture. Moisture interferes with both the formation and stability of the perovskite phase. Perovskite precursor solutions, typically dissolved in polar solvents, may interact with water molecules to form intermediate complexes that fail to transition into the desired perovskite phase. In addition, water can disrupt the bonding between lead halide octahedral and A-site cations, leading to the formation of hydrated perovskite compounds via hydrogen bonding. This interaction alter the Pb–X–Pb bond angles, affecting orbital hybridization between Pb and X atoms and thus the energy levels and photophysical properties of charge carriers [6–8]. To mitigate moisture-induced degradation, various approaches have been investigated, including modifying halide chemistry with pseudohalides such as thiocyanate (SCN^-), formate ($HCOO^-$), superhalogens (BF_4^- , PF_6^-) [9–11], which exhibit stronger interactions with Pb^{2+} compared to iodide, mitigating moisture-induced disruption and enhancing the environmental stability of PSCs. Additionally, our previous studies have highlighted the critical influence of solvent properties on air-processed perovskite films. Moisture alters the surface tension of precursor solutions, often resulting in poor film coverage during deposition [12,13]. Rapid heating strategies have been shown to effectively counteract moisture effects by enabling quick solidification and crystallization [14]. However, while these methods produce high film coverage, they typically result in small-grained perovskite films with significant boundary defects, which compromise device performance and stability.

Sequential deposition offers a promising alternative fabrication approach, as it decouples the solidification and crystallization steps, eliminating the requirement for anti-solvent treatment [15,16]. This method involves initially depositing an inorganic layer, such as lead iodide (PbI_2), followed by a reaction with an organic solution. Sequential deposition enables precise control over the composition and chemical properties of the precursors, promoting efficient crystallization. For example, in methylammonium lead iodide ($MAPbI_3$), the reaction involves the crystallization of partially amorphous PbI_2 , followed by intercalation and structural reorganization with methylammonium iodide (MAI). This mechanism reveals the advantage of sequential deposition on the perovskite crystallization [17]. The viability of air-processed sequential deposition was first demonstrated by Tai et al., who replaced PbI_2 with $Pb(SCN)_2$ as the inorganic precursor. The resulting films, fabricated by reacting $Pb(SCN)_2$ with MAI, achieved a pinhole-free perovskite film and a PCE of 15.12% in [18]. More recently, mixed-cation perovskites incorporating cesium (Cs) and formamidinium (FA) have exhibited improved thermal stability and performance compared to $MAPbI_3$. However, the composition and processing of the mixed-cation systems are more complex, requiring precise optimization to achieve good quality films and high performance. Liu et al. reported that controlled humidity exposure during mixed-cation perovskite fabrication facilitated quasi-solid-solid reactions, enhancing a spatially homogeneous intermediate phase via promoted mass diffusion of organic salts [19]. However, excessive humidity led to the formation of hydrated perovskite phases, larger grains, and poor film uniformity, reducing device performance. These results indicate that the precise control of the environmental conditions is required for the fabrication of air-processed perovskite layers due to the narrow process window. Nevertheless, there is still a lack of detailed and effective procedures for fabricating air-processed mixed-cation perovskite layers.

In this work, we successfully developed an air-processable mixed-cation perovskite layer using sequential deposition, addressing the challenges caused by moisture through targeted strategies. Initially, control devices with optimized mixed-cation perovskite layers were fabricated in a nitrogen glovebox. Subsequently, the sequential deposition process was transferred into ambient air. To improve the film coverage, a pre-heating substrate was employed to reduce the surface tension of the precursor solutions in air, significantly improving film coverage. During the reaction between the inorganic and organic layers, moisture-induced issues were mitigated using two strategies: the removal of moisture from the isopropanol (IPA) solvent to prevent α -phase degradation of formamidinium lead iodide ($FAPbI_3$), and the introduction of imidazole iodide (ImI) into the PbI_2 precursor. The ImI molecules strongly coordinated with Pb sites, effectively capping the Pb sites and blocking moisture interference. This ensured complete reaction with formamidinium iodide (FAI) without residual PbI_2 . These combined strategies enabled the fabrication of PSCs with an air-processed mixed-cation perovskite layers achieving a PCE of 18.73%. Moreover, stability testing illustrated that PSCs incorporating ImI exhibited a T80 lifetime exceeding 500 h, demonstrating the potential of air-processable perovskite layers for scalable and efficient photovoltaic applications.

2. Methods

2.1. Materials

Nickel acetate tetrahydrate ($\text{Ni}(\text{CH}_3\text{COO})_2 \cdot 4\text{H}_2\text{O}$, 99.0%) was purchased from Showa Chemical (Tokyo, Japan). Poly(3-hexylthiophene-2,5-diyl) derivative (P3HT-COOH, $M_w \sim 90\text{K}$) was purchased from Rieke Metals, (Lincoln, NE, USA). Ethanolamine (EA, 99%) was obtained from Acros Organics, (Carlsbad, CA, USA). Formamidinium Iodide (FAI, 99.99%), Imidazolium iodide (ImI, 99.99%), and Methylammonium chloride (MACl, 99.99%) were purchased from Greatcell solar materials, (Queanbeyan, Australia). Cesium Iodide (CsI, 99.99%), Dimethyl sulfoxide (DMSO, 99.9%), Dimethylformamide (DMF, $\geq 99.9\%$), Chlorobenzene (CB, 99.9%), Isopropanol (IPA, 99.5%), Polyethyleneimine (PEI, branched, Average M_n 10k), and ethanol (EtOH, 99.8%) were purchased from Sigma-Aldrich, (St. Louis, MO, USA). Lead iodide (PbI_2 , 99.999%) was purchased from TCI, (Tokyo, Japan). All the chemicals were used without further purification. 2-Thiopheneethylamine, hydrochloride (TEACl) was synthesized following by the previous study. Briefly, 2-(aminomethyl)thiophene (98%, Tokyo Chemical Industry Co., Ltd.) and hydrochloric acid (36.5–38.0%, Sigma-Aldrich) were mixed (mole ratio 1:1.05) and stirred in an ice bath for 2h. The excess solvent in the resultant solution was thereafter removed by using a rotary evaporator. The bright yellow powder of the product was collected in a vial bottle and washed with diethyl ether (DEE) three times. Then recrystallization with ethanol to further purify the reactant. Finally, the TEACl was placed in a vacuum condition for 12 h and then stored in N_2 atmosphere.

2.2. Preparation of Precursor Solutions

For the sol-gel NiO_x solution, 0.124 mg nickel acetate tetrahydrate was dissolved in 1 mL of ethanol, and then the solution was stirred at 60 °C until it became clear. After adding 30 μL of ethanolamine, the solution was filtered with 0.22 μm poly(1,1,2,2-tetrafluoroethylene) (PTFE). For the P3HT-COOH solution 0.5 mg P3HT-COOH powder was dissolved in 1 mL of DMF. For the 1.3 M inorganic solution, the PbI_2 with 5 mol% CsI were dissolved into DMF:DMSO (9:1 vol%). For ImI doping, the different ImI concentrations were dissolved in inorganic solution. The solution was then stirred at 70 °C until overnight. The organic salt solution, FAI, MACl (63 mg:7 mg), dissolved into 1 mL of IPA. TEACl was dissolved in IPA at a concentration of 4 mM. The PCBM was used as the electron transporting layer (ETL) with the concentration of 20 mg ml^{-1} in CB. Work function modifier (WFL) was prepared in IPA with the PEI concentration of 0.1 wt%.

2.3. Device Fabrication for Perovskite Solar Cells

The p-i-n device structure was adopted as FTO/ NiO_x /P3HT-COOH/Perovskite/TEACl/PCBM/PEI/Ag, which according to the previous work [20]. The fluorine doped tin oxide (FTO) coated glass substrates (TEC7, Hartford) were washed by ultrasonic bath for 15 min using detergent solution, methanol, and isopropanol, respectively. The substrates were blown dry with nitrogen, then treated with UV-Ozone for 15 min. The NiO_x and P3HT-COOH were prepared in air. For NiO_x film, a 50 μL volume of sol-gel NiO_x solution was spin-coated onto the substrate at 4000 rpm for 20 s and annealed at 300 °C for 30 min to complete crystallization. Next, a P3HT-COOH layer was spin-coated onto the NiO_x film using 50 μL of solution at 4000 rpm for 20 s, followed by annealing at 140 °C for 10 min. The perovskite layer was prepared using sequential deposition, with control devices fabricated in N_2 . For the N_2 -processed inorganic layer, a 50 μL volume of inorganic solution was spin-coated onto the substrate at 3000 rpm for 30 s and annealed at 70 °C for 1 min. For the air-processable inorganic layer, the substrate was pre-heated to the target temperature before spin-coating 50 μL of inorganic solution at 3000 rpm for 30 s, followed by annealing at 70 °C for 1 min. The organic layer, whether prepared in N_2 or air, was formed by spin-coating 75 μL of organic salt solution onto the inorganic layer at 3000 rpm for 30 s, followed by annealing at 100 °C for 15 min. Subsequent layers were prepared in a nitrogen glovebox. For passivation layer, the TEACl solution was spin-coated at 3000 rpm for 20 s onto the perovskite layer and then thermally annealed at 70 °C for 15 min. Then, the 50 μL of PCBM solution and 50 μL of PEI solution were spin-coated on the film at 1000 rpm for 30 s and 3000 rpm for 30 s, respectively in nitrogen. Then, 100 nm of silver electrodes was deposited on the top of WF layer with an active area of 0.09 cm^2 by using thermal evaporation.

2.4. Materials and Devices Characterization

Measurements were performed using a voltage source meter (Keithley 2410, Keithley Instrument, Solon, OH, USA) under an AM 1.5G solar simulator with irradiation at 100 mW cm^2 . The X-ray diffraction (XRD) patterns were obtained using X-ray diffractometer (Bruker D8 Discover A25, Bruker AXS GmbH, Karlsruhe, Germany) under $\text{Cu K}\alpha$ radiation ($\lambda = 1.5406 \text{ \AA}$). The scanning range was set from 5° to 50°, with a step size of 0.01°. The

total beam exposure time was approximately 8 min. The absorption spectra was measured by using optical spectroscopy (V750, JASCO, Tokyo, Japan)

3. Results and Discussion

Before examining the effects of environmental conditions, it is essential to establish a reliable sequential deposition method for the control sample. In this study, the control perovskite layer was fabricated using sequential deposition in a nitrogen glovebox. This method involves depositing the inorganic material first to form a structural scaffold, followed by the introduction of an organic solution to complete the solid-liquid phase reaction required for perovskite phase formation. The perovskite composition used was FAPbI₃, prepared from two precursor solutions containing PbI₂ and FAI, respectively. The solid-liquid phase reaction of perovskite relies on a balance between reaction kinetics and solution penetration. Rapid phase reactions can result in perovskite formation on the surface of the PbI₂ scaffold before the solution fully infiltrates the deeper layers, leaving unreacted PbI₂ at the bottom of the scaffold. Such an incomplete reaction adversely affects device performance and compromises the phase stability of the α -FAPbI₃ phase [21,22]. The unreacted PbI₂ in the perovskite layer may further degrade the device performance and phase stability of the α -FAPbI₃ [23]. To mitigate these issues, various molar ratios of cesium iodide (CsI) were incorporated into the PbI₂ precursor at concentrations of 5%, 10%, 15%, and 20%. The performances and J-V curves of the PSCs are shown in Table 1 and Figure 1a. For pristine condition, the PSCs exhibited an average PCE of $7.53 \pm 0.89\%$, with an average open-circuit voltage (V_{oc}) of 1.01 V, an average short-circuit current density (J_{sc}) of $16.85 \pm 1.01 \text{ mA/cm}^2$, and an average fill factor (FF) of $45.41 \pm 3.07\%$. Introducing 5 mol% CsI significantly improved the average PCE of PSCs to $14.06 \pm 0.85\%$, driven by increases in average FF of $69.61 \pm 3.46\%$ and J_{sc} of $20.14 \pm 0.37 \text{ mA/cm}^2$. However, further increasing the CsI concentration to 10 mol% resulted in a decline in PCE of PSCs due to reductions in both FF and J_{sc} . The results indicate that 5 mol% CsI is the optimal doping concentration for PSCs. Figure 1b illustrates the X-ray diffraction (XRD) analysis of perovskite films with varying CsI concentrations. The FAPbI₃-based perovskite crystal structure exhibited a light-absorbed α -phase, characterized by peaks at (111) of 13.9° and (012) of 19.7° , and a non-light-absorbed δ -phase at (010) of 11.8° and (011) of 16.3° [24]. The pristine perovskite primarily shows δ -phase peaks with minor α -phase peaks, indicating a phase transition from α -phase to δ -phase and corresponding to poor device performance. After 5 mol% CsI doping, the perovskite film exhibited an increased α -phase peaks with a slight PbI₂ and δ -phase peak. The Cs doping of perovskite stabilized the α -phase, and improved the PCE of the PSCs. At higher CsI concentrations (>15 mol%), the α -phase peaks diminished, and a δ -CsPbI₃ peak appeared at 10° , indicating a phase transition caused by excessive doping [25]. This suggests that a mismatch in the tolerance factor plays a critical role, demonstrating that while moderate CsI doping effectively suppresses phase transition, excessive doping induces instability [26].

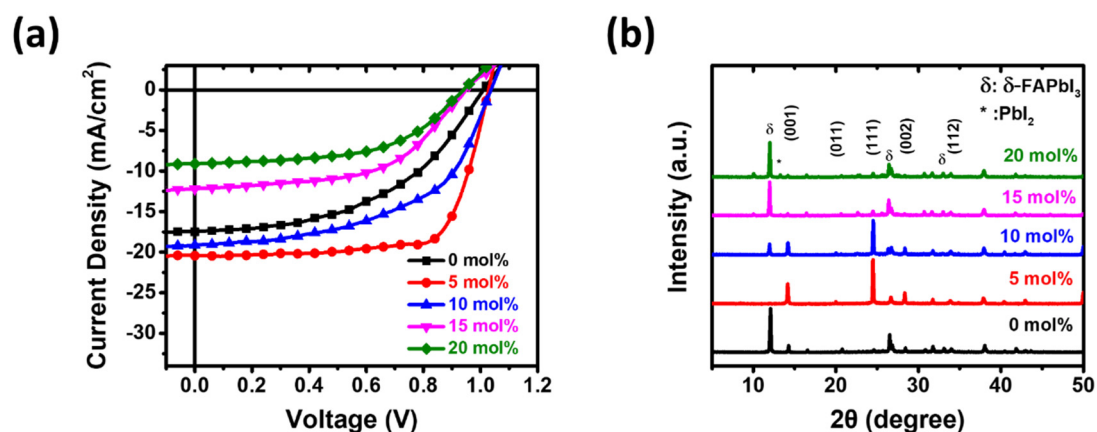


Figure 1. (a) J-V curves of PSCs, and (b) XRD patterns of perovskite films with varying CsI concentrations.

Table 1. Performance of PSCs prepared using perovskite films with varying CsI concentrations.

CsI Concentration (mol%)	V_{oc} (V)	J_{sc} (mA/cm ²)	FF (%)	PCE _{avg} (%)	PCE _{highest} (%)
0	1.00 ± 0.01	16.85 ± 1.01	45.40 ± 3.07	7.52 ± 0.89	8.20
5	1.03 ± 0.01	20.14 ± 0.37	69.61 ± 3.46	14.06 ± 0.85	14.82
10	1.02 ± 0.03	17.32 ± 1.00	51.34 ± 1.52	8.79 ± 0.77	10.23
15	0.92 ± 0.05	8.77 ± 2.02	57.40 ± 1.98	4.5 ± 1.00	6.08
20	0.93 ± 0.03	6.53 ± 1.38	56.14 ± 3.56	3.3 ± 0.71	4.51

To develop air-processable perovskite films, we first prepared the inorganic layer in air while keeping the organic coating process within a nitrogen atmosphere. The performance and J-V curves of the PSCs are presented in Table 2 and Figure 2a. PSCs fabricated from the air-processable inorganic layer exhibited a significantly reduced average PCE of $0.61 \pm 1.07\%$, compared to an average PCE of $14.38 \pm 2.03\%$ for pristine PSCs. Figure 2b displays the absorption spectra of the perovskite films. Compared to pristine perovskite films, the perovskite film prepared using the air-processable inorganic layer exhibited absorption characteristics of non-light-absorbing δ -phase and lacked the desired α -phase. This result reflects the poor quality of the air-processed inorganic layer, consistent with its film appearance. The poor coating quality in air is attributed to moisture, which attaches to the substrate, increasing the surface tension and contact angle and thereby reducing film coverage [27]. To address this, a pre-heating method was employed to reduce surface tension by providing additional energy to the solvent, promoting effective spreading. Substrates were pre-heated at various temperatures (40, 50, 60, 70, and 80 °C) for 5 min to ensure thermal equilibrium before spin coating. The device performance and statistical PCE distribution of PSCs fabricated with inorganic layers prepared at different pre-heating temperatures are shown in Table 3 and Figure 3. At 40 °C, the average PCE of PSCs improved significantly from $0.61 \pm 1.07\%$ (Table 2) to $9.34 \pm 3.35\%$, indicating successful deposition of the PbI_2 film and its subsequent reaction to form the perovskite phase. However, thinner inorganic films tend to facilitate a more complete perovskite phase conversion but often leave unreacted organic salts, such as FAI, within the perovskite film. These residual ions are prone to photo-induced phase segregation under illumination, leading to a decline in device performance [28]. As the temperature increased to 70 °C, the device performance increased to the average PCE of $16.42 \pm 1.64\%$ due to the improvement of FF. Beyond the pre-heating temperature, 80 °C, the average PCE decreased to $8.41 \pm 3.90\%$, likely due to incomplete perovskite conversion resulting from an excessively thick inorganic film (~ 727 nm). At higher pre-heating temperatures, the solvent not only spreads more effectively but also evaporates more rapidly, resulting in thicker films. These results demonstrate that the effectiveness of pre-heating method, particularly at 70 °C, in addressing coating challenges associated with preparing inorganic layers in air, enabling significant improvements in perovskite film quality and device performance.

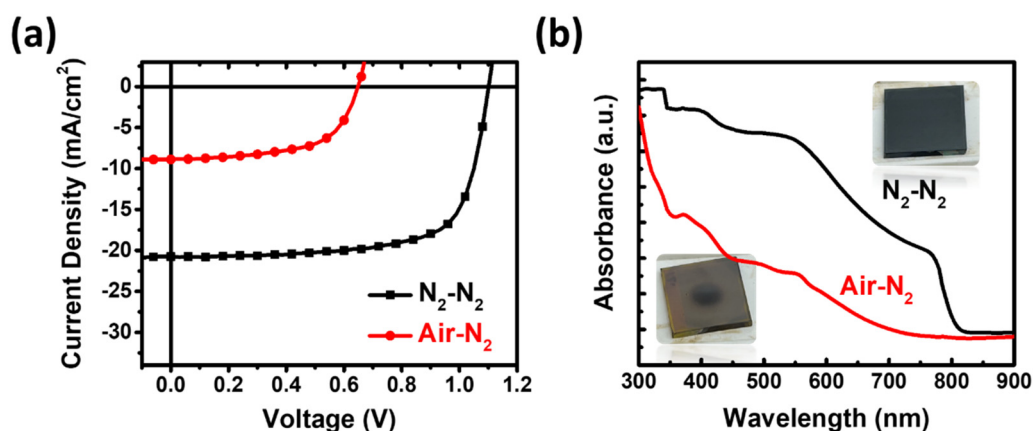
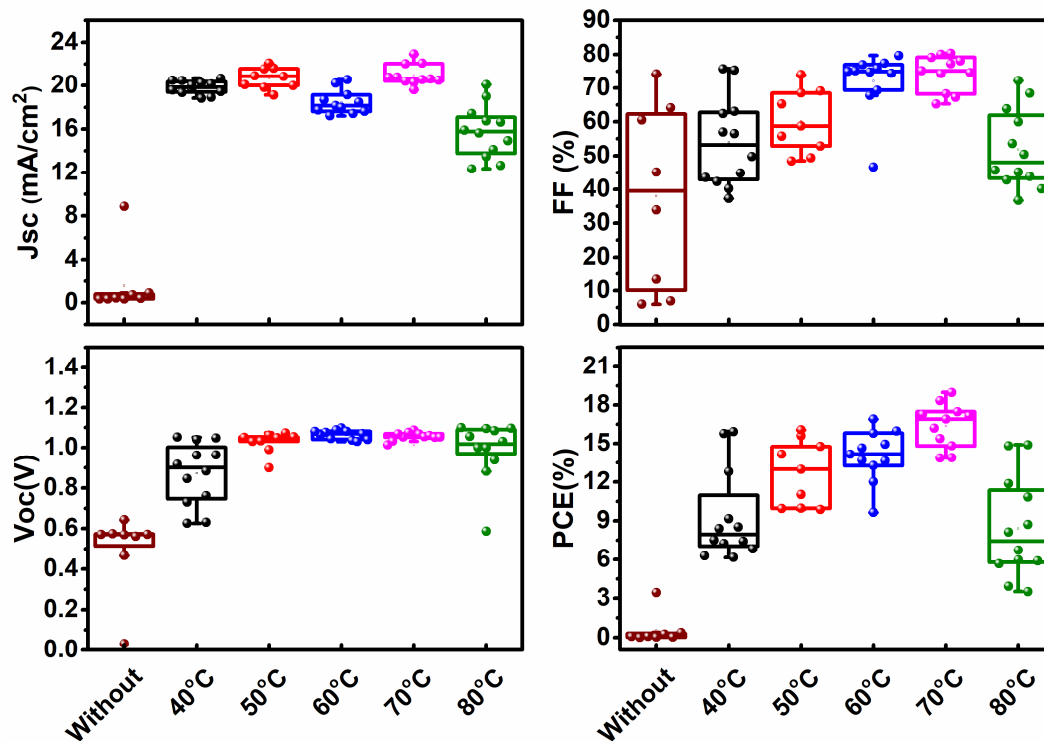
**Figure 2.** (a) J-V curves of PSCs, and (b) absorption spectra of perovskite films with the inorganic layer prepared in N₂ and air.

Table 2. Device performance of PSCs with the inorganic layer prepared in N₂ and air.

Preparation of Inorganic Layer	V _{oc} (V)	J _{sc} (mA/cm ²)	FF (%)	PCE _{avg} (%)	PCE _{highest} (%)
N ₂	1.08 ± 0.03	20.74 ± 0.38	64.7 ± 7.22	14.38 ± 2.03	16.09
Air	0.53 ± 0.16	1.51 ± 2.55	54.77 ± 32.96	0.61 ± 1.07	3.44

**Figure 3.** Performance distributions of PSCs with inorganic layers prepared at different pre-heating temperatures.**Table 3.** Device performance of PSCs with inorganic layers prepared at different pre-heating temperatures.

Pre-Heating Temperature [°C]	V _{oc} (V)	J _{sc} (mA/cm ²)	FF (%)	PCE _{avg} (PCE _{highest}) (%)	Thickness (nm)	
					Inorganic Films	Perovskite Films
40	0.87 ± 0.14	19.82 ± 0.58	53.99 ± 12.62	9.34 ± 3.35 (15.91)	347.6 ± 7.3	467.6 ± 9.4
50	1.03 ± 0.05	20.67 ± 0.91	60.21 ± 8.80	12.70 ± 2.40 (16.05)	464.3 ± 18.5	512.6 ± 11.3
60	1.06 ± 0.02	18.47 ± 1.05	72.06 ± 8.66	14.04 ± 1.91 (16.88)	539.3 ± 10.2	611.2 ± 17.5
70	1.06 ± 0.02	20.92 ± 0.93	74.69 ± 05.11	16.42 ± 1.64 (18.95)	562.1 ± 29.7	655.3 ± 19.0
80	0.99 ± 0.14	15.74 ± 2.41	51.88 ± 11.67	8.41 ± 3.90 (14.89)	727.5 ± 17.7	735.6 ± 36.3

For the organic layer deposition in air, precise control of the solid-liquid phase reaction is critical. The organic solution, prepared using isopropanol (IPA), is highly susceptible to moisture due to the polar nature of IPA, which makes it highly miscible with water. After several hours of exposure to air, the initially colorless solution turned bright yellow, as shown in Figure 4a. The color change is attributed to the formation of triiodide (I₃⁻), which is a byproduct of moisture-induced oxidation of iodide ions [29,30]. The presence of I₃⁻ reduces the reactivity of the organic solution, compromising its suitability in forming high quality perovskite layers. Therefore, effective

moisture prevention strategies are essential. Here, we proposed reducing the moisture content in the input materials by adding molecular sieves into the IPA before the organic solution preparation. This method effectively trapped moisture, stabilizing the iodide ions and maintaining the colorless state of the organic solution, unlike the yellowing observed in untreated solutions. We further used XRD analysis (Figure 4b) to confirm that the perovskite films prepared with the treated IPA exhibited strong α -phase peaks, whereas films prepared with untreated IPA primarily showed δ -phase peaks. This result aligns with the visual observation of the perovskite films (Figure 4a). The pristine perovskite film decomposed rapidly, exhibiting a yellowish appearance, while those prepared using treated IPA retained a stable brown-to-dark coloration. These results reveal the importance of moisture control in maintaining the quality and stability of perovskite films formed through organic layer deposition in air.

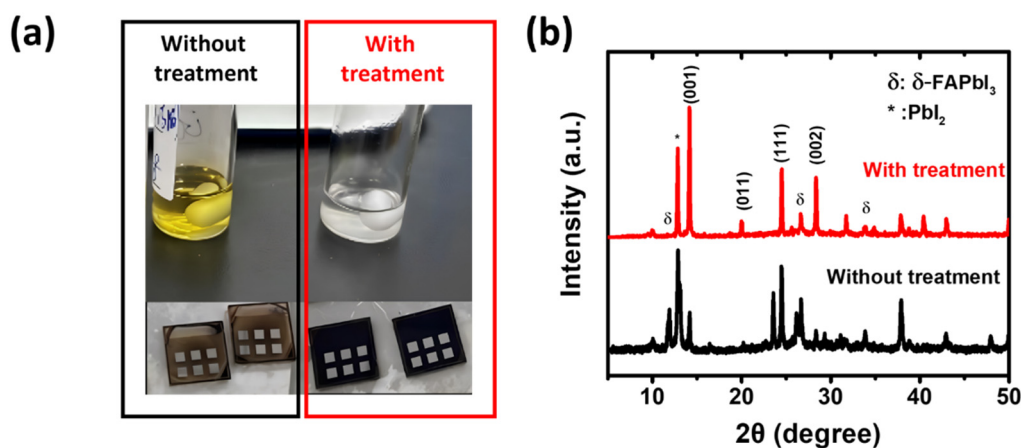


Figure 4. (a) Photos of the organic precursor solution and perovskite films prepared using the IPA with and without moisture-trapped treatment. (b) XRD patterns of perovskite films.

For the organic coatings prepared in air, the air-processable PbI_2 successfully transitioned entirely to the perovskite phase, including the α -phase and reduced δ -phase, as confirmed by the XRD analysis in Figure 4b. However, the residual PbI_2 peak observed during the perovskite phase transition indicates incomplete conversion, which is particularly affected by moisture. Moisture interferes with the reaction by reducing the availability of halide reactants, thereby hindering the complete transition to the perovskite phase. While moisture prevention strategies and solution modifications are essential, controlling perovskite crystallization is also crucial for achieving a complete phase transition. The reaction mechanism between the inorganic layer and organic components begins with the intercalation of organic molecules into the layered inorganic structure, followed by the formation of the 3D perovskite framework [31]. In the presence of moisture, water molecules interfere with this intercalation process by disrupting the interactions between alkylamine cations and other ions. This accelerates degradation and results in residual PbI_2 . To address this issue, imidazole iodide (ImI), which contains two nitrogen (N) atoms, was introduced into the inorganic solution, as shown in Figure 5a. The imidazolium functional group in ImI , with its positively charged N^+ site, enhances the reaction by attracting halide ions, thereby facilitating the perovskite phase transition. Figure 5b presents the XRD analysis of the inorganic layers with varying ImI concentrations (0, 1, 3, 5, 20 mol%). ImI molecules exhibit strong coordination with the inorganic layer, as evidenced by studies on intermediate formation [32,33]. This coordination alters the lattice structure of PbI_2 , leading to a noticeable shift in its XRD peaks. The shift confirms the interaction between ImI and the inorganic layer. However, at higher ImI concentrations (e.g. 20 mol%), a small peak appeared before 10° , corresponding to the formation of a low-dimensional perovskite phase, which suggests that excessive ImI disrupts the perovskite structure. Figure 5c illustrates the XRD analysis of the perovskite films with varying ImI concentrations. The addition of ImI significantly reduced the intensity of the PbI_2 peak while increasing the intensity of the α -phase, indicating that ImI effectively facilitates the perovskite phase transition in air. However, at higher ImI concentrations, the strong interaction between ImI and PbI_2 appeared to interfere with the perovskite phase transition. Based on these findings, 5 mol% ImI was identified as the optimal concentration, striking a balance between promoting phase transition and avoiding structural disruption, to achieve an efficient and stable phase transition in air.

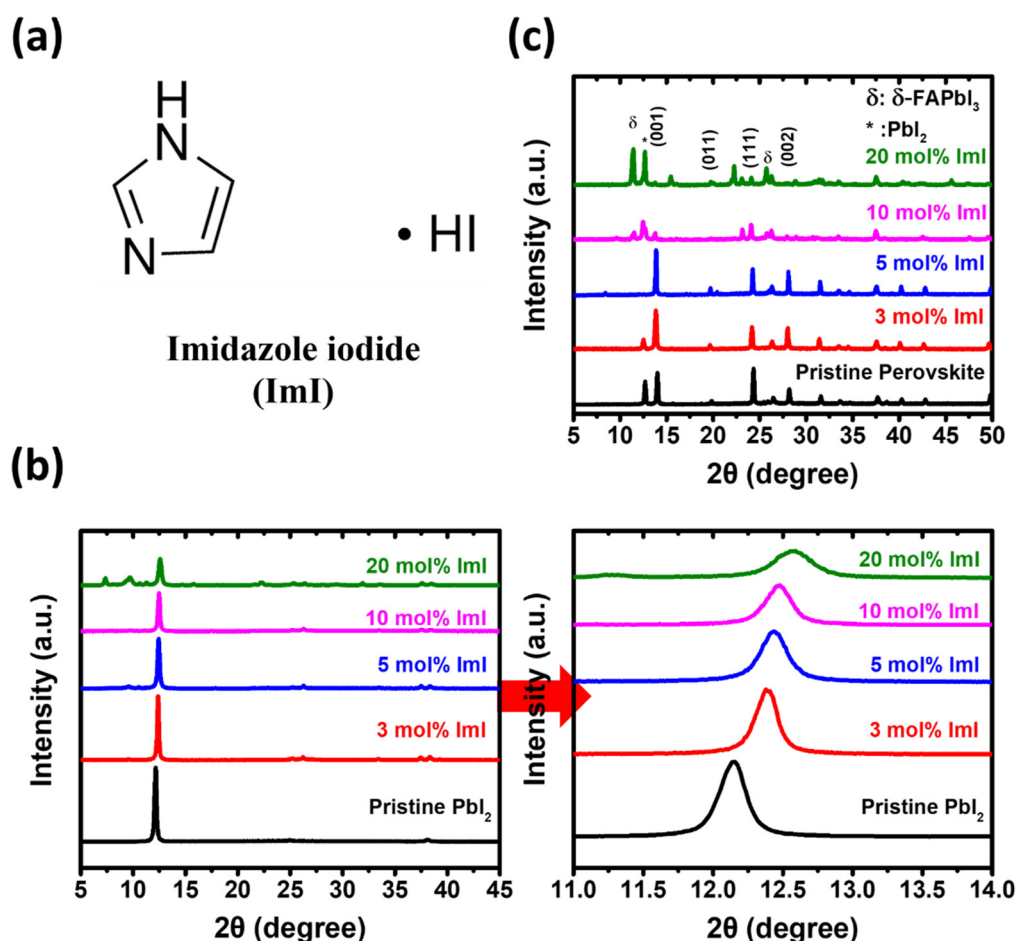


Figure 5. (a) the chemical structure of ImI. (b) XRD patterns of inorganic layers with varying ImI concentrations. (c) XRD patterns of perovskite films with varying concentrations of ImI.

The performance distributions of PSCs with and without ImI are summarized in Table 4 and depicted in Figure 6. The incorporation of ImI into PbI_2 resulted in a narrower performance distribution compared to pristine PSCs, indicating that ImI effectively facilitates the perovskite phase transition in air. The J-V curves of the champion PSCs with and without ImI are presented in Figure 7a. The champion PSC with 5 mol% ImI achieved a PCE of 18.73%, with a V_{oc} of 1.10V, a J_{sc} of 23.01 mA/cm^2 , and a FF of 74.06%. In contrast, the pristine PSC exhibited a PCE of 14.52%, with a V_{oc} of 1.04 V, a J_{sc} of 19.31 mA/cm^2 , and a FF of 72.80%. Further, the stability of PSCs was also evaluated under dark storage in a glovebox without encapsulation, as shown in Figure 7b. The PSCs with 5 mol% ImI demonstrated a T_{80} lifetime exceeding 500 h, significantly outperforming the control PSC, which showed the T_{80} lifetime of merely 180 h. The results suggest the dual benefits of ImI incorporation, as its defect passivation effect not only enhances the device performance but also markedly improves long-term stability of PSCs fabricated in air.

Table 4. Performance of PSCs prepared using inorganic layers with various concentration of ImI.

ImI (mol%)	V_{oc} (V)	J_{sc} (mA/cm^2)	FF (%)	PCE_{avg} (%)	$\text{PCE}_{highest}$ (%)
0	1.01 ± 0.08	18.81 ± 0.97	61.87 ± 8.44	11.74 ± 2.44	14.52
5	1.05 ± 0.02	21.26 ± 1.43	74.60 ± 3.84	16.50 ± 1.91	18.73

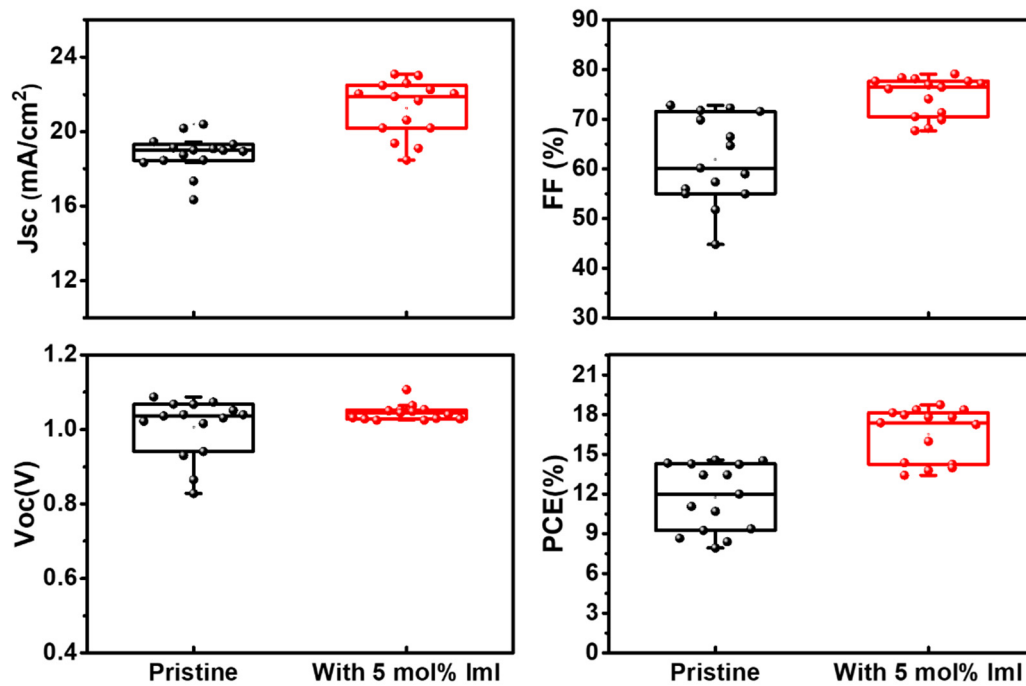


Figure 6. Devices distribution of PSCs prepared using inorganic layers with and without ImI.

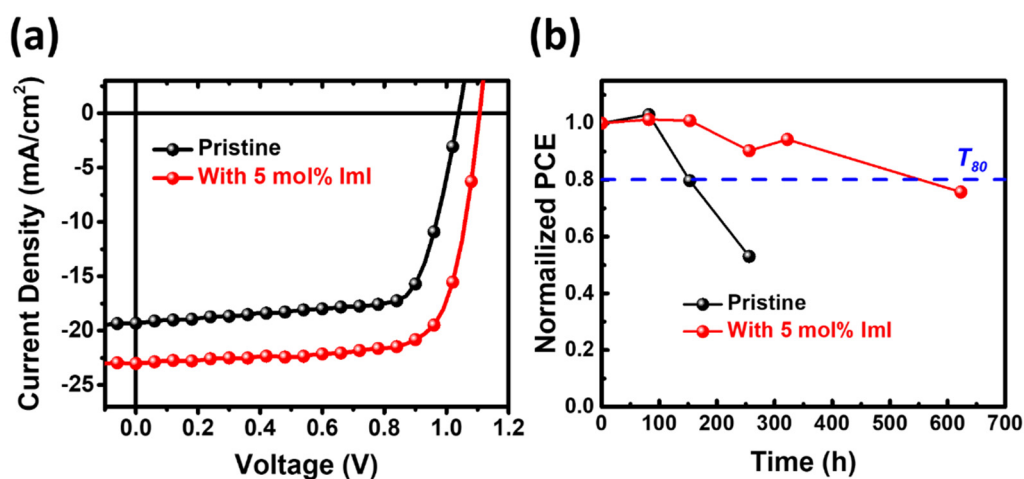


Figure 7. (a) J-V curves of champion PSCs, (b) stability test of PSCs prepared using inorganic layers with and without ImI.

4. Conclusions

This study successfully demonstrates the development of an air-processable perovskite layer using sequential deposition, addressing the challenges of moisture interference through targeted strategies. By optimizing the fabrication process, including pre-heating substrates to reduce surface tension, and introducing ImI as an additive to the PbI_2 precursor, we significantly improved the perovskite film quality and performance of the perovskite solar cells. The strong coordination of ImI effectively mitigated moisture-induced reactions, enhanced α -phase formation, and eliminated residual PbI_2 , enabling an efficient phase transition even under ambient conditions. The PSCs achieved the highest PCE of 18.73%, representing a notable improvement over the control devices. Furthermore, stability testing revealed that the inclusion of ImI extended the T_{80} lifetime to over 500 h, highlighting its role in defect passivation and enhanced durability. These findings demonstrate the effectiveness of ImI in addressing moisture-related challenges during perovskite film deposition and its potential for enabling scalable, air-processed PSC fabrication. The results pave the way toward the commercial viability of perovskite-based photovoltaic.

Author Contributions

S.-H.H.: Methodology, Validation, Investigation, Formal analysis, Data Curation, Writing—Original Draft. C.-T.T.: Validation, Investigation, Formal analysis, Data Curation. Y.-H.H.: Validation, Investigation, Formal analysis. C.-F.L.: Validation, Investigation, Formal analysis. Y.-R.C.: Formal analysis, Data Curation. Y.-C.H.: Conceptualization, Resources, Writing—Review & Editing, Supervision, Project administration, Funding acquisition. W.-F.S.: Conceptualization, Supervision. All authors have read and agreed to the published version of the manuscript.

Funding

Financial support provided by the National Science and Technology Council of Taiwan (Grant Nos. NSTC 111-2923-E-002-012-MY3; 111-2923-E-002-007-MY3, NSTC 112-2628-E-131-001-MY4, NSTC 111-2221-E-182-040-MY3, NSTC 113-2622-E-131-006-, and NSTC113-2221-E-003-001) and Chang Gung University (URRPD2N0011) are highly appreciated.

Data Availability Statement

The datasets generated during and/or analyzed during the current study are available from the corresponding author upon reasonable request.

Conflicts of Interest

All authors declare no financial or non-financial conflict of interest.

References

1. Im, J.-H.; Lee, C.-R.; Lee, J.-W.; et al. 6.5% efficient perovskite quantum-dot-sensitized solar cell. *Nanoscale* **2011**, *3*, 4088–4093.
2. Huang, Z.; Bai, Y.; Huang, X.; et al. Anion- π interactions suppress phase impurities in FAPbI₃ solar cells. *Nature* **2023**, *623*, 531–537.
3. Park, N.-G. Perovskite solar cells: An emerging photovoltaic technology. *Mater. Today* **2015**, *18*, 65–72.
4. Jeon, N.J.; Noh, J.H.; Kim, Y.C.; et al. Solvent engineering for high-performance inorganic-organic hybrid perovskite solar cells. *Nat. Mater.* **2014**, *13*, 897–903.
5. Yang, M.; Li, Z.; Reese, M.O.; et al. Perovskite ink with wide processing window for scalable high-efficiency solar cells. *Nat. Energy* **2017**, *2*, 17038.
6. Prasanna, R.; Gold-Parker, A.; Leijtens, T.; et al. Band Gap Tuning via Lattice Contraction and Octahedral Tilting in Perovskite Materials for Photovoltaics. *J. Am. Chem. Soc.* **2017**, *139*, 11117–11124.
7. Egger, D.A.; Kronik, L. Role of Dispersive Interactions in Determining Structural Properties of Organic-Inorganic Halide Perovskites: Insights from First-Principles Calculations. *J. Phys. Chem. Lett.* **2014**, *5*, 2728–2733.
8. Zhou, L.; Neukirch, A.J.; Vogel, D.J.; et al. Density of States Broadening in CH₃NH₃PbI₃ Hybrid Perovskites Understood from ab Initio Molecular Dynamics Simulations. *ACS Energy Lett.* **2018**, *3*, 787–793.
9. Chen, J.; Kim, S.-G.; Park, N.-G. FA_{0.88}CS_{0.12}PbI₃-(PF₆) Interlayer Formed by Ion Exchange Reaction between Perovskite and Hole Transporting Layer for Improving Photovoltaic Performance and Stability. *Adv. Mater.* **2018**, *30*, 1801948.
10. Jeong, J.; Kim, M.; Seo, J.; et al. Pseudo-halide anion engineering for α -FAPbI₃ perovskite solar cells. *Nature* **2021**, *592*, 381–385.
11. Zhang, W.; Saliba, M.; Moore, D.T.; et al. Ultrasoft organic-inorganic perovskite thin-film formation and crystallization for efficient planar heterojunction solar cells. *Nat. Commun.* **2015**, *6*, 6142.
12. Huang, S.-H.; Tian, K.-Y.; Huang, H.-C.; et al. Controlling the Morphology and Interface of the Perovskite Layer for Scalable High-Efficiency Solar Cells Fabricated Using Green Solvents and Blade Coating in an Ambient Environment. *ACS Appl. Mater. Interfaces* **2020**, *12*, 26041–26049.
13. Li, C.-F.; Huang, H.-C.; Huang, S.-H.; et al. High-Performance Perovskite Solar Cells and Modules Fabricated by Slot-Die Coating with Nontoxic Solvents *Nanomaterials* [Online], 2023.
14. Huang, S.-H.; Guan, C.-K.; Lee, P.-H.; et al. Toward All Slot-Die Fabricated High Efficiency Large Area Perovskite Solar Cell Using Rapid Near Infrared Heating in Ambient Air. *Adv. Energy Mater.* **2020**, *10*, 2001567.
15. Kulkarni, S.A.; Baikie, T.; Boix, P.P.; et al. Band-gap tuning of lead halide perovskites using a sequential deposition process. *J. Mater. Chem. A* **2014**, *2*, 9221–9225.
16. Chen, H. Two-Step Sequential Deposition of Organometal Halide Perovskite for Photovoltaic Application. *Adv. Funct. Mater.* **2017**, *27*, 1605654.

17. Ummadisingu, A.; Grätzel, M. Revealing the detailed path of sequential deposition for metal halide perovskite formation. *Sci. Adv.* **2018**, *4*, e1701402.
18. Tai, Q.; You, P.; Sang, H.; et al. Efficient and stable perovskite solar cells prepared in ambient air irrespective of the humidity. *Nat. Commun.* **2016**, *7*, 11105.
19. Liu, K.; Luo, Y.; Jin, Y.; et al. Moisture-triggered fast crystallization enables efficient and stable perovskite solar cells. *Nat. Commun.* **2022**, *13*, 4891.
20. Glowienka, D.; Huang, S.-H.; Lee, P.-H.; et al. Understanding the Dominant Physics Mechanisms on the p-i-n Perovskite Solar Cells Fabricated by Scalable Slot-Die Coating Process in Ambient Air. *Sol. RRL* **2024**, *8*, 2300791.
21. Wang, H.; Ye, F.; Liang, J.; et al. Pre-annealing treatment for high-efficiency perovskite solar cells via sequential deposition. *Joule* **2022**, *6*, 2869–2884.
22. Xu, Q.; Shi, B.; Li, Y.; et al. Diffusible Capping Layer Enabled Homogeneous Crystallization and Component Distribution of Hybrid Sequential Deposited Perovskite. *Adv. Mater.* **2024**, *36*, 2308692.
23. Lin, D.; Gao, Y.; Zhang, T.; et al. Vapor Deposited Pure α -FAPbI₃ Perovskite Solar Cell via Moisture-Induced Phase Transition Strategy. *Adv. Funct. Mater.* **2022**, *32*, 2208392.
24. Stoumpos, C.C.; Malliakas, C.D.; Kanatzidis, M.G. Semiconducting Tin and Lead Iodide Perovskites with Organic Cations: Phase Transitions, High Mobilities, and Near-Infrared Photoluminescent Properties. *Inorganic Chem.* **2013**, *52*, 9019–9038.
25. Montecucco, R.; Quadrivi, E.; Po, R.; et al. All-Inorganic Cesium-Based Hybrid Perovskites for Efficient and Stable Solar Cells and Modules. *Adv. Energy Mater.* **2021**, *11*, 2100672.
26. Li, Z.; Yang, M.; Park, J.-S.; et al. Stabilizing Perovskite Structures by Tuning Tolerance Factor: Formation of Formamidinium and Cesium Lead Iodide Solid-State Alloys. *Chem. Mat.* **2016**, *28*, 284–292.
27. Cheng, Y.; Xu, X.; Xie, Y.; et al. 18% High-Efficiency Air-Processed Perovskite Solar Cells Made in a Humid Atmosphere of 70% RH. *Solar RRL* **2017**, *1*, 1700097.
28. Yoon, S.J.; Kuno, M.; Kamat, P.V. Shift Happens. How Halide Ion Defects Influence Photoinduced Segregation in Mixed Halide Perovskites. *ACS Energy Lett.* **2017**, *2*, 1507–1514.
29. Philippe, B.; Park, B.-W.; Lindblad, R.; et al. Chemical and Electronic Structure Characterization of Lead Halide Perovskites and Stability Behavior under Different Exposures—A Photoelectron Spectroscopy Investigation. *Chem. Mat.* **2015**, *27*, 1720–1731.
30. Yu, X.; Qin, Y.; Peng, Q. Probe Decomposition of Methylammonium Lead Iodide Perovskite in N₂ and O₂ by in Situ Infrared Spectroscopy. *J. Phys. Chem. A* **2017**, *121*, 1169–1174.
31. Meng, K.; Wang, X.; Xu, Q.; et al. In Situ Observation of Crystallization Dynamics and Grain Orientation in Sequential Deposition of Metal Halide Perovskites. *Adv. Funct. Mater.* **2019**, *29*, 1902319.
32. Węclawik, M.; Gağor, A.; Piecha, A.; et al. Synthesis, crystal structure and phase transitions of a series of imidazolium iodides. *CrystEngComm* **2013**, *15*, 5633–5640.
33. Weber, O.J.; Marshall, K.L.; Dyson, L.M.; et al. Structural diversity in hybrid organic–inorganic lead iodide materials. *Acta Crystallogr. Sect. B* **2015**, *71*, 668–678.